Determination of the elastic and stiffness characteristics of cross-laminated timber plates from flexural wave velocity measurements

Andrea Santoni[a,*], Stefan Schoenwald[b], Bart Van Damme[b], Patrizio Fausti[a]

[a] *Engineering Department, University of Ferrara, via G. Saragat 1, 44122 Ferrara, Italy*
[b] *Laboratory for Acoustics and Noise Control, Empa - Swiss Federal Laboratories for Material Science and Technology, Ueberlandstrasse 129, CH-8600 Dübendorf, Switzerland*

Abstract

Cross-laminated timber (CLT) is an engineered wood with good structural properties and it is also economically competitive with the traditional building construction materials. However, due to its low volume density combined with its high stiffness, it does not provide sufficient sound insulation, thus it is necessary to develop specific acoustic treatments in order to increase the noise reduction performance. The material's mechanical properties are required as input data to perform the vibro-acoustic analyses necessary during the design process. In this paper the elastic constants of a CLT plate are derived by fitting the real component of the experimental flexural wave velocity with Mindlin's dispersion relation for thick plates, neglecting the influence of the plate's size and boundary conditions. Furthermore, its apparent elastic and stiffness properties are derived from the same set of experimental data, for the plate considered to be thin. Under this latter assumption the orthotropic behaviour of an equivalent thin CLT plate is described by using an elliptic model and verified with experimental results.

Keywords: orthotropic plate, stiffness properties, elastic constants, wavenumber analysis, dispersion relation, thin/thick plate

1. Introduction

Cross-laminated timber, often abbreviated to the acronym CLT, is an engineered solid wood material consisting of an odd number of layers of wooden beams glued together, alternating perpendicularly the orientation of the fibres of each ply. CLT building panels are generally fabricated with three, five, or seven layers, according to the static requirements, with a total thickness up to 500 mm. According to the standard EN 16351 [1] the thickness of each layer should be within the range $4 - 65$ mm. The success of CLT plates has continuously been increasing in the building construction market over the last twenty years. Its high strength, good structural stability, fulfilment of safety requirements together with the cost competitiveness and the possibility to rapidly assemble prefabricated panels, make CLT a valuable alternative to traditional

*Corresponding author
Email address: andrea.santoni@unife.it (Andrea Santoni)

Article accepted in Journal of Sound and Vibration; *10 April 2017*

Published article available online: https://doi.org/10.1016/j.jsv.2017.04.018

building construction materials such as concrete, masonry and steel. However, due to their high stiffness combined with their low density, CLT structures do not provide satisfactory noise reduction. Therefore, in order to improve sound insulation performance, it is necessary to design and optimize specific acoustic treatments, such as additional layers applied to the walls [2], like gypsum board linings on a cavity, or a concrete floating screed over the CLT floor structures [3]. Most of the prediction methods to compute structure-borne and air-borne sound transmission require the geometric characteristics of building elements and the materials' mechanical properties as input data, in addition to some acoustic descriptors. Since many wood species with different mechanical characteristics can be used to manufacture CLT structures, an easily implementable non-destructive procedure to evaluate the elastic and stiffness properties would be beneficial for a straightforward characterization of specific CLT building elements. The literature offers a variety of different approches to experimentally investigate the mechanical properties of solid wood through non destructive tests [4]. Many of them are modal analysis-based methods [5, 6], or involve ultrasound measurements [7, 8]. The experimental approch presented here is based on wave propagation analysis within the audible frequency range. The flexural wave velocity can be directly evaluated by measuring the time-of-flight difference between two adjoining transducers in line with the excitation source, a technique derived from ultrasound measurements [9] and also applied for the characterization of visco and poro-elastic materials [10]. Alternatively, the structural wavenumber can be determined by measuring the phase difference between two consecutive accelerometers, as proposed by Rindel [11] for low frequency measurements. This approach has also been applied by Nightingale [12] to study a wooden joist floor, implementing a slightly different setup in order to investigate higher frequencies. A method to compute the phase velocity, based on phase difference of the frequency response function FRF between two transducers [13], was also applied by Thwaites to detect damages in sandwich structures, other than to determine the material's elastic properties [14]. While these approaches uses continuous wave random noise excitation or impact impulses, the method to be described here involves short pulse excitation. Pulse excitation usually requires more effort during the measurement stage, since a longer time is needed to investigate a wide frequency range, compared to broadband excitation. On the other hand, it allows one to obtain accurate results with a much easier signal processing. The novelty aspect of the proposed method is represented by an analytical data fitting of the experimental wave velocity in order to diminish the number of single frequencies to be tested within the investigated band, reducing significantly the measurement time. Besides, the fitting procedure also limits the influence of the scatter in the experimental data, especially at high frequencies.

The aim of this work is to present a fast and non-destructive method to investigate the elastic and stiffness properties of particular orthotropic elements using wave propagation analysis. The dynamic behaviour of CLT plates is known to be orthotropic [15, 16], therefore the elastic parameters, and the stiffness properties, are direction dependent. The wave velocity has to be evaluated for many angles over the plate surface to analyse separately the propagation along different directions. The propagation velocity of flexural waves has been measured on a three-ply cross-laminated timber plate surface for different propagation angles, instead of cutting beams along those directions [17]. Consequently, due to its non-destructive nature, the method can be applied either in-situ or in laboratory. The study was motivated by the necessity to investigate the vibro-acoustic behavior of CLT plates. In structural design CLT elements are generally treated as multilayered structures, or composite liminates, and analysed using advanced plate theories [18]. Even though elementary Kirchhoff's or Mindlin's theories, might not be enough accurate for structural analysis of CLT plates and higher order approach are necessary, they allow accurate

Published article available online: https://doi.org/10.1016/j.jsv.2017.04.018

approximated results when applied in vibro-acoustic modelling, since the order of magnitude of the transverse displacements induced in the structures is much smaller. An example of how they have been used to model sound radiation efficiency of a CLT plate can be found in [19]. In the next paragraph the dispersion relation for flexural waves propagating in a plate is introduced, highlighting the differences between Kirchhoff's classical thin plate theory and Mindlin's theory for thick plates. In Paragraph 3 the tested structure and the measurements setup are introduced, and the signal processing to determine the real part of the flexural wave velocity is described. The methods to evaluate the material's stiffness characteristics are presented in Paragraph 4. From the experimental wavenumbers the stiffness properties of the equivalent thin orthotropic plate have been derived. Moreover, it was also possible to evaluate the in-plane elastic constants of the orthotropic plate under Mindlin's assumptions. The main results are finally shown and discussed in Paragraph 5.

2. Theoretical background

The velocity of a flexural wave propagating in an elastic solid depends on the frequency. The wave dispersion relation can be determined from the equation of motion of the vibrating structure. There are several simplified analytical approaches to describe the dynamic response of a beam or a plate. Kirchhoff's plate theory, also known as classical thin plate theory, considers only pure bending, neglecting both rotational inertia and shear deformation effect. Under these assumptions, the equation of motion of a thin isotropic plate undergoing unforced vibration is described as a function of the transverse displacement w as [20]:

$$D\nabla^4 w + \rho h \frac{\partial^2 w}{\partial t^2} = 0. \tag{1}$$

The bending wavenumber k_B depends on the angular frequency ω, the bending stiffness of the plate D, given in Eq. (11), its density ρ, and its thickness h:

$$k_B = \sqrt[4]{\frac{\rho h \omega^2}{D}}. \tag{2}$$

The thin plate assumptions are generally valid for frequencies with a bending wavelength satsfying the relationship: $\lambda_B > 2\pi h$. When this assumption is not fulfilled, rotational inertia and shear deformation have a significant effect on the plate's dynamic response and need to be considered. The equation of motion for free vibrations of a thick isotropic plate of constant thickness h, derived using Mindlin's approximation [21], may be written as:

$$D\nabla^4 w - \left[\frac{\rho D}{\kappa^2 G} + I\right]\nabla^2 \frac{\partial^2 w}{\partial t^2} + \rho \frac{I}{\kappa^2 G}\frac{\partial^2 w}{\partial t^2} + \rho h \frac{\partial^2 w}{\partial t^2} = 0, \tag{3}$$

where $I = \rho h^3/12$ indicates the mass moment of inertia of the plate and G is the plate's shear modulus. The coefficient κ^2, similarly to Timoshenko shear coefficient in thick beam theory [22], takes into account that the shear stress is not constant over the plate thickness. It can be approximated using a simple relationship, that follows from some considerations about the phase velocity limit of large wavenumbers [23], as:

$$\kappa = \frac{c_R}{c_S} = \frac{0.87 + 1.12\nu}{1 + \nu}, \tag{4}$$

Published article available online: https://doi.org/10.1016/j.jsv.2017.04.018

where c_S is the pure shear wave velocity and c_R represents the Rayleigh surface velocity. Mindlin's dispersion relation is obviously more complicated than the simple Kirchhoff classical thin plate theory and for a rectangular plate it is given in terms of wave velocities by [24]:

$$\left(1-\frac{c^2}{\kappa^2 c_S^2}\right)\left(\frac{c_L^2}{c^2}-1\right)=\frac{12}{h^2\left(\frac{\omega}{c}\right)^2}, \tag{5}$$

where c represents the flexural wave velocity, while the speed of longitudinal c_L and shear waves c_S can be determined from the plate's elastic modulus E and Poisson's ratio ν, its density ρ, and its shear modulus G:

$$\begin{cases} c_L = \sqrt{\frac{E}{\rho(1-\nu^2)}} & \text{: longitudinal wave velocity;} \\ \\ c_S = \sqrt{\frac{G}{\rho}} & \text{: pure shear wave velocity.} \end{cases}$$

The dispersion relation for pure bending, derived from thin plate theory, shows an unlimited increase of the phase velocity with frequency. However, the velocity for large wavenumbers should be limited, due to rotational inertia and especially shear deformation. According to Mindlin's theory, at low frequencies the flexural wave velocity corresponds to the phase velocity of a pure bending wave, while at high frequencies, in case of an in-phase motion of the opposite surfaces of the plate [25], it approaches the Rayleigh surface velocity $c_R = \kappa c_S$. A comparison between thin and thick plate dispersion relations is plotted in Figure 1. Mindlin's dispersion

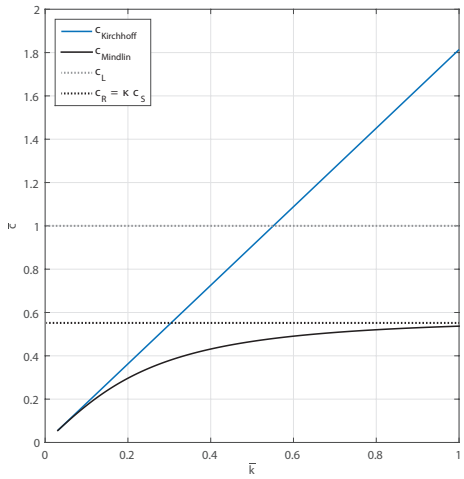

Figure 1: Comparison between thin plate and thick plate wave velocity dispersion curves. The normalised wave velocity: $\bar{c} = c/c_L$ is plotted against the normalised wavenumber: $\bar{k} = kh/2\pi$.

relation, given in Eq. (5), was derived for an infinite plate, therefore, the influence of boundary conditions and structure's dimensions is neglected. It should be stressed that the transverse

Published article available online: https://doi.org/10.1016/j.jsv.2017.04.018

displacement of a thick plate is not caused only by pure bending, as in thin plates, but at high frequencies the contribution of in-plane and shear waves becomes significant. In the following, for simplicity's sake, the expression flexural wave will be address to indicate the structural waves inducing transverse displacement in thick plates and real structures, while bending wave will be used referring to thin plate approximation.

So far a homogeneous isotropic plate has been considered. However, orthotropic materials, with different elastic properties along mutually perpendicular directions, are often used in building constructions, aerospace or automotive industry and many other fields of engineering. In some structures this peculiar behaviour can be caused by the presence of ribs or stiffeners and it is common to treat such elements as equivalent orthotropic plates. Yet some materials present a natural orthotropy due to their inner structure, or to their layered geometry, like CLT plates. The constitutive relations for an orthogonally orthotropic material make use of nine elastic constants and are given in the compliance form as:

$$\begin{Bmatrix} \varepsilon_x \\ \varepsilon_y \\ \varepsilon_z \\ \varepsilon_{xy} \\ \varepsilon_{xz} \\ \varepsilon_{yz} \end{Bmatrix} = \begin{bmatrix} \frac{1}{E_x} & -\frac{\nu_{yx}}{E_y} & -\frac{\nu_{zx}}{E_z} & 0 & 0 & 0 \\ -\frac{\nu_{xy}}{E_x} & \frac{1}{E_y} & -\frac{\nu_{zy}}{E_z} & 0 & 0 & 0 \\ -\frac{\nu_{xz}}{E_x} & -\frac{\nu_{yz}}{E_y} & \frac{1}{E_z} & 0 & 0 & 0 \\ 0 & 0 & 0 & \frac{1}{2G_{xy}} & 0 & 0 \\ 0 & 0 & 0 & 0 & \frac{1}{2G_{xz}} & 0 \\ 0 & 0 & 0 & 0 & 0 & \frac{1}{2G_{yz}} \end{bmatrix} \begin{Bmatrix} \sigma_x \\ \sigma_y \\ \sigma_z \\ \sigma_{xy} \\ \sigma_{xz} \\ \sigma_{yz} \end{Bmatrix}. \tag{6}$$

The velocity of a vibrational wave propagating into a solid element depends upon the material elastic characteristics; therefore in an orthotropic plate, it depends on the propagation direction. A method to experimentally determine the elastic properties of an orthotropic panel is proposed in the next section.

3. Experimental setup

The frequency-dependent velocity of a flexural wave, propagating in a cross-laminated timber plate, was experimentally determined. The three-ply CLT plate investigated is 4.2 m wide and 2.9 m high, and its total thickness is 80 mm: the outer layers are approximately 30 mm thick, while the inner core thickness is 20 mm. The propagating waves were induced into the plate with a B&K 4809 vibration exciter driven by short sinusoidal pulses (2.5 cycles). The central frequency was varied from 100 Hz to 3100 Hz at 40 Hz steps. The transverse acceleration was measured by five PCB-353B15 accelerometers (10 mV/g) aligned with the excitation point and equally spaced 10 cm apart, as sketched in Figure 2. In order to avoid the influence of the vibrational near field, and to consider only the propagating wave neglecting the evanescent component, the closest accelerometer was placed 50 cm from the excitation point. According to Cremer et al. [26] the evanescent near-field is usually considered negligible at a distance greater than half the structural wavelength from the discontinuity. However, it was not possible to know a priori this wavelength. Thus the 50 cm span was chosen in order to balance the distance of the transducers from all the discontinuities of the plate: namely the excitation point and the edges. The signals were generated and acquired by a National Instruments data acquisition system controlled with an in-house implemented software. Each measurement was performed for 5 different angles, from 0 to $\pi/2$ radians, to investigate the dependency of the wave velocity upon the propagation direction.

Published article available online: https://doi.org/10.1016/j.jsv.2017.04.018

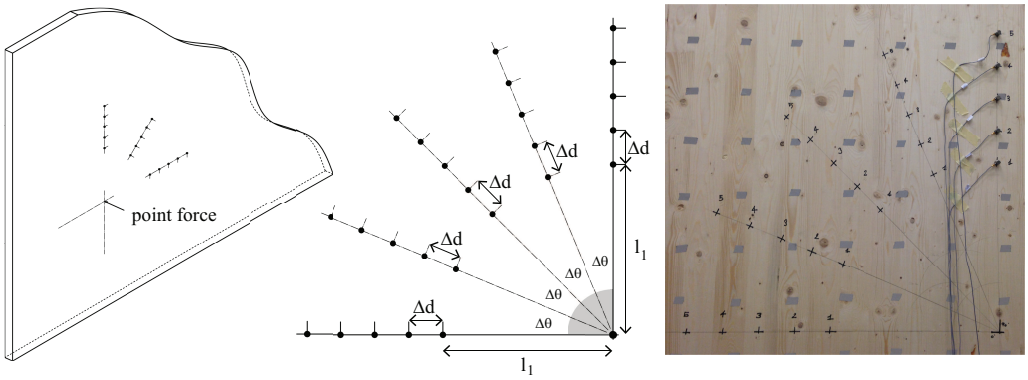

Figure 2: Experimental setup for different propagation angles at steps of $\Delta\theta = \pi/8$. The first measurement position is placed at a minimum distance $l_1 = 50$ cm from the excitation point to avoid near field effects and the accelerometers are equally spaced: $\Delta d = 10$ cm.

To evaluate the phase velocity of lateral displacement each set of measured data was analysed with two different methods. The wave velocity can be determined by evaluating the phase difference between each pair of adjoining transducers. In order to consider only the direct incoming wave the measured signals must be windowed, in time domain, removing reflections from the edges. However, the time window should be long enough allowing the propagating wave to reach the furthest measurement point. Due to the dispersive nature of the bending wave it is appropriate to shrink the time window as the frequency increases, since the length of the signal reduces. The window size is thus determined for each investigated frequency as a function of the first positive peak of the incomining pulse, detected in the time domain. A clear description of the window size effects on the measurements can be found in [27], where the phase difference method was used to investigate the stiffness properties of building components. The phase difference is evaluated between each pair of consecutive accelerometers, by performing an FFT on the windowed signals. For each frequency the real part of the bending wavenumber, hence the wave velocity, can be evaluated by dividing the measured phase shift $\Delta\phi$ by the transducers spacing Δd, and averaging over n accelerometer positions:

$$\mathrm{Re}\left\{k_B\left(\omega\right)\right\} = \frac{1}{n-1}\sum_{i=1}^{n-1}\left(-\frac{\Delta\phi_{i,i+1}}{\Delta d_{i,i+1}}\right), \tag{7}$$

$$\mathrm{Re}\left\{c_B\left(\omega\right)\right\} = \frac{\omega}{\mathrm{Re}\left\{k_B\left(\omega\right)\right\}}. \tag{8}$$

In the second method, the wave velocity is determined directly from the time of flight difference between neighbouring accelerometers. The measured data were first smoothed by applying a second order Savitzky-Golay polynomial filter in order to have a better signal to noise ratio, then the time of arrival of the first positive peak was determined for each acceleration signal. The time of flight is evaluated as the difference between the arrival time of two consecutive accelerometers: $\Delta t_{i,i+1} = t_{i+1} - t_i$. Assuming the dissipation to be negligible for small distances, the real part of the wave velocity is given by the ratio of the spacing $\Delta d_{i,i+1}$, between the transducers i and $i+1$,

Published article available online: https://doi.org/10.1016/j.jsv.2017.04.018

to the related time of flight $\Delta t_{i,i+1}$, averaged over $(n-1)$ pairs of neighbouring accelerometers:

$$\mathrm{Re}\left\{c_B\left(\omega\right)\right\} = \frac{1}{n-1}\sum_{i=1}^{n-1}\left(\frac{\Delta d_{i,i+1}}{\Delta t_{i,i+1}}\right). \tag{9}$$

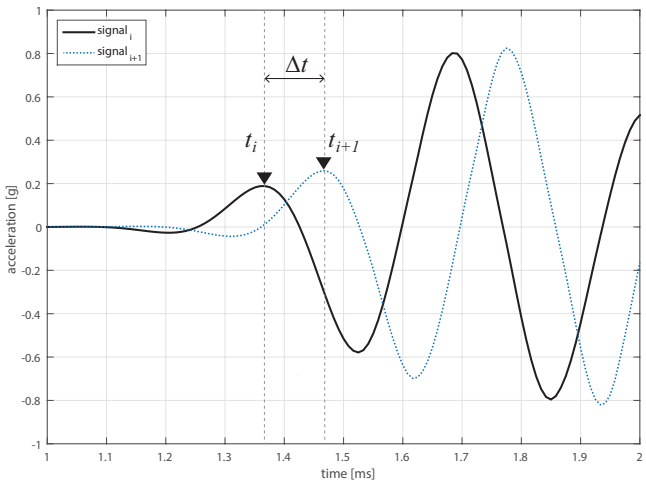

Figure 3: Evaluation of the time of flight of the propagating wave between two consecutive measurement positions: $f = 3100$ Hz – $\theta = \pi/2$.

An example of the determination of the time of flight difference between a pair of consecutive transducers is given in Figure 3. Both methods assume that all the reflections are removed from the signal by the time window and that the imaginary part of the wave velocity is negligible. It is clear from the standard deviations of the measured data, plotted in Figure 4(a) as an example and reported in Appendix A for all the investigated directions, that the phase difference method is more reliable in the low-mid frequency range. On the other hand, the results obtained from the time of flight differences are more appropriate at high frequencies to reduce the spread of the measured values. The spacing between the transducers should be much smaller than the bending wavelength to correctly evaluate the phase shift between the signals to apply the first method. The two data sets were therefore combined using a cut-off frequency: $f_{co} = 1500$ Hz, determined by minimising the overall error, computed for each investigated frequency by summing the experimental deviation of all the investigated directions.

4. Experimental wavenumber analysis

The measured wave velocities were fitted to obtain continuous smooth curves within the frequency range $50 - 5000$ Hz using Mindlin's dispersion relation given in Eq. (5). A fitting algorithm, based on non-linear regression, was implemented in Matlab R2014b, using Mindlin's dispersion relation as input model in the `nlinfit` function. It returns the estimated coefficients,

Published article available online: https://doi.org/10.1016/j.jsv.2017.04.018

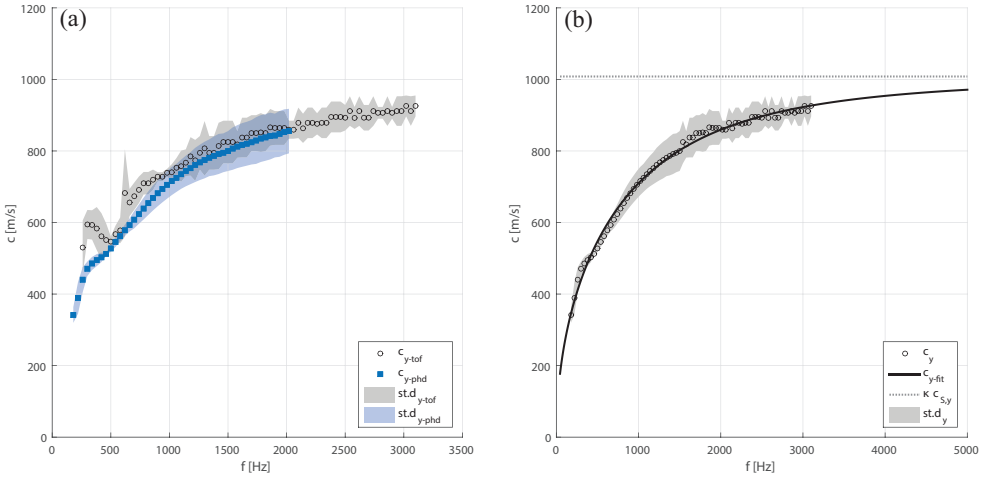

Figure 4: (a) – Experimental wave velocity determined from the phase difference (*phd*) and the time of flight (*tof*) methods. (b) – Curve fitting of the experimental wave velocity using Mindlin's dispersion relation. The shaded area represents the standard deviation of measured data. Propagation angle: $\theta = \pi/2$.

c_L and c_S, for which the model function best fits the measured values. The fitted curves agree very well with the experimental data, as shown in Figure 4(b) and in Appendix A. Moreover the fitting method proved to be efficient, since the final results are independent from the used initial guess value, even if the frequency step in the measured data vector is increased from 40 Hz to 160 Hz, as shown in Figure 5.

4.1. Apparent elastic properties: thin orthotropic plate

4.1.1. Principal directions x-y

Solving the equations of motion for an orthotropic thick plate, under Mindlin's assumptions, requires a great effort [28]. Sometimes, for engineering applications, simplified approaches are preferred over the more sophisticated ones. Even if these simplified theories do not rigorously describe the structure dynamics, they provide accurate approximated results in a relatively short computational time. The apparent frequency dependent bending stiffness of an equivalent thin orthotropic plate was derived from the experimental wave velocity measured along the principal directions. Using Kirchhoff's theory, which neglects both the rotatory inertia and the shear deformation effect, the equation of motion of an orthotropic plate, lying in the $x - y$ plane with the principal directions oriented along the Cartesian axes, is given by [29]:

$$D_x \frac{\partial^4 w}{\partial x^4} + 2B \frac{\partial^4 w}{\partial x^2 \partial y^2} + D_y \frac{\partial^4 w}{\partial y^4} + \rho h \frac{\partial^2 w}{\partial t^2} = 0, \tag{10}$$

where D_x and D_y is the apparent bending stiffness along the principal directions:

$$D_x = \frac{E_x h^3}{12\left(1 - \nu_{xy}\nu_{yx}\right)}; \qquad D_y = \frac{E_y h^3}{12\left(1 - \nu_{xy}\nu_{yx}\right)}; \tag{11}$$

Published article available online: https://doi.org/10.1016/j.jsv.2017.04.018

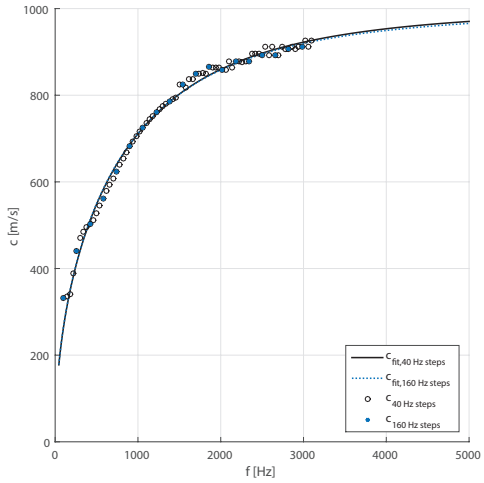

Figure 5: Comparison between wave velocity curves obtained by fitting the experimental data, measured at steps of 40 Hz and of 160 Hz, within the frequency range 100 Hz to 3100 Hz. Propagation angle: $\theta = \pi/2$.

and B is the effective torsional stiffness defined as:

$$B = \frac{\nu_{xy} D_y}{2} + \frac{\nu_{yx} D_x}{2} + 2G_{xy}\frac{h^3}{12} \approx \sqrt{D_x D_y}. \tag{12}$$

The approximation of the effective torsional stiffness B is only valid under the simplifying assumption that the in-plane shear modulus G_{xy} is a function of the elastic moduli along the principal directions and the plate's Poisson's ratio [30]:

$$G_{xy} = \frac{\sqrt{E_x E_y}}{2\left(1 + \sqrt{\nu_{xy}\nu_{yx}}\right)}. \tag{13}$$

The apparent frequency-dependent elastic properties along the principal directions E_x and E_y can be easily estimated from the experimental wave velocity $c_{exp,\theta}$ and the thin plate dispersion relation, given in Eq. (2), as:

$$\begin{aligned} E_x &= \frac{12\rho c_{exp,x}^4\left(1-\nu^2\right)}{h^2\omega^2}, \\ E_y &= \frac{12\rho c_{exp,y}^4\left(1-\nu^2\right)}{h^2\omega^2}. \end{aligned} \tag{14}$$

It should be noted that ν_{xy} and ν_{yx} are elastic constants corresponding to the structure configuration [31] and the Poisson's ratio is assumed to be $\nu = \sqrt{\nu_{xy}\nu_{yx}} = 0.3$, as typical for wood materials.

4.1.2. Direction dependent elastic properties: elliptic model

To account for the orthotropic behaviour of the CLT plate a well-established elliptic model [32, 33] is adopted assuming the wavenumbers along the principal directions to be independent.

Published article available online: https://doi.org/10.1016/j.jsv.2017.04.018

For any propagation angle θ the bending wavenumber $k_B(\theta)$ is derived from the data measured along the x-direction ($\theta = 0$) and the y-direction ($\theta = \pi/2$) as:

$$k_B(\theta) = \sqrt{k_{B,x}^2(\theta) + k_{B,y}^2(\theta)}; \tag{15}$$

$$\begin{aligned} k_{B,x}(\theta) &= k_{B,x}\cos\theta, \\ k_{B,y}(\theta) &= k_{B,y}\sin\theta. \end{aligned} \tag{16}$$

The orthotropic plate's bending stiffness, like the structural wavenumber, is direction dependent and it is defined as:

$$D(\theta) = D_x\cos^4\theta + 2B\cos^2\theta\sin^2\theta + D_y\sin^4\theta. \tag{17}$$

Computing the orthotropic bending stiffness using Eq. (17) would require the knowledge of the in-plane shear modulus G_{xy}. Alternatively the direction dependent bending stiffness might be approximated for each propagation angle θ as a function of the orthotropic wavenumber $k_B(\theta)$ obtained from Eq. (15):

$$D(\theta) = \frac{\rho h\omega^2}{k_B^4(\theta)}. \tag{18}$$

4.2. Elastic constants: thick orthotropic plate

As pointed out in the previous section, the simplifying assumptions of Kirchhoff's classical plate theory, which disregards the influence of rotatory inertia and shear deformation, need to be compensated by considering frequency dependent material elastic properties. A more sophisticated approach to investigate the plate dynamics, like Mindlin's thick plate theory, requires a greater effort and longer computational time, but it allows to derive the material elastic constants. The resulting coefficients of the fitting algorithm represent the plate longitudinal and shear waves velocities. From the values of c_L and c_S it is possible to derive directly the elastic modulus $E(\theta)$ and the shear modulus $G(\theta)$ for all the investigated propagation directions:

$$E_\theta = \rho c_{L,\theta}^2\left(1-\nu^2\right), \tag{19}$$

$$G_{\theta z} = \rho c_{S,\theta}^2. \tag{20}$$

The bending stiffness along the principal directions D_x and D_y can be computed using the same formulation given for a thin plate in Eq. (11), while the in-plane shear modulus G_{xy} can be approximated according to Eq. (14).

It should be recalled that the dynamic properties of elastic materials always present, to some extent, a frequency dependency; which might be significant, like in highly damped elastomers, or negligible in low damped materials like steel, concrete, and wood. A complex modulus is often used in vibro-acoustic analysis to characterise the material's elastic and damping properties. Even though the method here proposed allows only to determine the real part of the complex dynamic modulus, the storage modulus E, its imaginary part E_l, sometimes called loss modulus, can be determined as a function of the plate loss factor η:

$$\overline{E} = E(1+\mathrm{i}\eta) = E + \mathrm{i}E_l \tag{21}$$

where $\overline{E}$ is the complex elastic modulus and $\mathrm{i} = \sqrt{-1}$ represents the imaginary unit. The plate's loss factor η can be experimentally evaluated by means of different approaches [34]. Further, since the real dynamic modulus and the loss modulus are interrelated, the latter, or analogously the loss factor, can be reconstructed from the real part of the dynamic modulus, as clearly explained by Pritz [35].

Published article available online: https://doi.org/10.1016/j.jsv.2017.04.018

5. Results and discussion

5.1. Material properties along the principal directions

The apparent parameters derived from the fitted wave velocity using the simplified thin plate dispersion relation are frequency dependent, as found in other studies when simplified assumptions are applied over more sophisticated theories for thick or composite plates [36, 37]. The frequency dependency of the apparent elastic modulus, or the apparent bending stiffness, takes into account that the plate dynamics at high frequencies is mostly governed by the shear deformation, which is neglected in classical thin plate theory. The apparent elastic moduli along the principal directions are plotted in Figure 6. The frequency dependent properties are compared with the elastic constant derived from the longitudinal wave velocity c_L resulting from the fitting algorithm, as described in section 4.2. Moreover, the shear moduli G_{xz} and G_{yz} were estimated

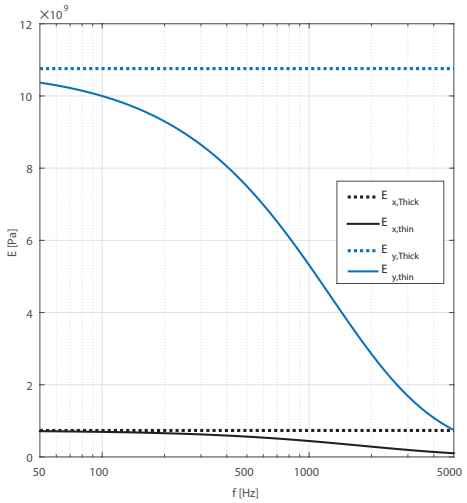

Figure 6: Comparison between the frequency dependent elastic properties of an equivalent thin orthotropic plate along the principal directions and the elastic constants derived using Mindlin's dispersion relation.

from the shear wave velocity c_S. The elastic and the shear moduli experimentally determined for different directions are reported in Table 1. The elastic and the shear moduli along the $x-$axis,

Table 1: CLT's elastic constants for different propagation angles.

θ [rad]	0	$\pi/8$	$\pi/4$	$3\pi/8$	$\pi/2$
E [Pa]	7.34e+08	9.68e+08	1.66e+09	3.80e+09	1.08e+10
G [Pa]	2.40e + 08	4.84e+08	2.52e+08	4.96e+08	5.72e+08

$\theta = 0$, have a comparable order of magnitude, while along the $y-$axis, $\theta = \pi/2$, the shear modulus

Published article available online: https://doi.org/10.1016/j.jsv.2017.04.018

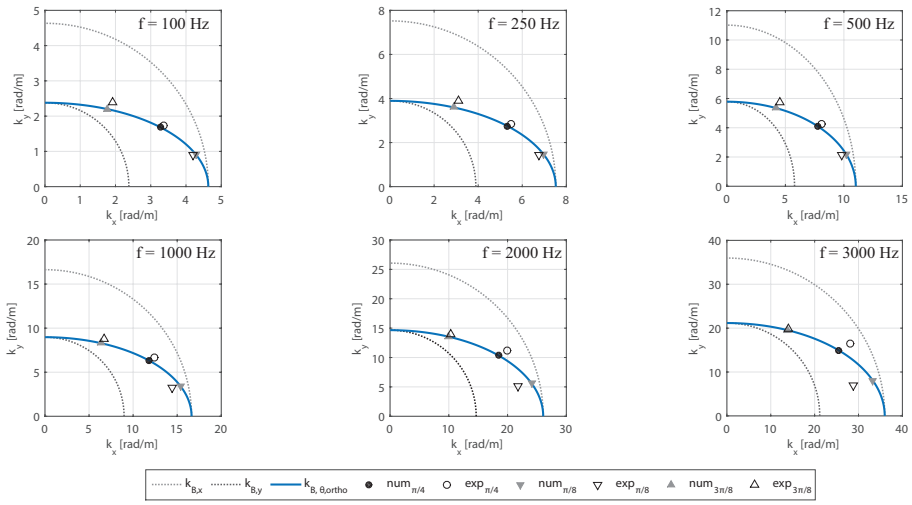

Figure 7: Elliptic model: comparison between the elliptic interpolation and the experimental wavenumbers, determined for the angles: $\pi/8$, $\pi/4$ and $3\pi/8$; at the frequencies: 100 Hz; 200 Hz, 500 Hz, 1000 Hz, 200 Hz and 3000 Hz.

is almost two orders of magnitude lower than the elastic modulus. For this reason, the equivalent elastic properties along this direction, as the frequency increases, exhibit a more emphasized reduction than in the opposite direction, and the same is obviously valid for the apparent bending stiffness. These findings agree very well with the results from a recent study performed on cross-laminated timber beams using a modal analysis approach [38].

5.2. Orthotropic elliptic model

To demonstrate the suitability of this approach for the investigated CLT plate, the theoretical bending wavenumbers obtained using the elliptic model were compared with the experimental values, for different propagation angles at various frequencies. This comparison between experimental and numerical data, given in Figure 7 in the wavenumber space, proves that the elliptic model is a reliable approximation to describe the orthotropic behaviour, showing a remarkably good agreement up to 1000 Hz. At higher frequencies the experimental wavenumbers slightly deviate from the predicted ellipse, consistent with the results of the analysis of wood material properties presented in [39]. Above 1000 Hz, the measured wavenumber along the $\theta = \pi/4$ direction is larger than the estimated value, whereas for $\theta = \pi/8$ the experimental wavenumbers is smaller than the numerical one. In other words, at high frequencies the elliptic model tends to overestimate the wave velocity propagating at $\theta = \pi/4$ while it underestimates the wave velocity along the direction $\theta = \pi/8$. However, it should be noted that in the high frequency range the standard deviation of the measured velocity is significantly higher and of the same order of magnitude as the difference between the experimental and estimated wavenumbers.

A similar comparison, with consistent results, is presented in Figure 8. The apparent bending stiffness approximated using Eq. (18), is compared with the values directly computed from the experimental wavenumber according to Eq. (2), for different angles, and at different frequencies.

Published article available online: https://doi.org/10.1016/j.jsv.2017.04.018

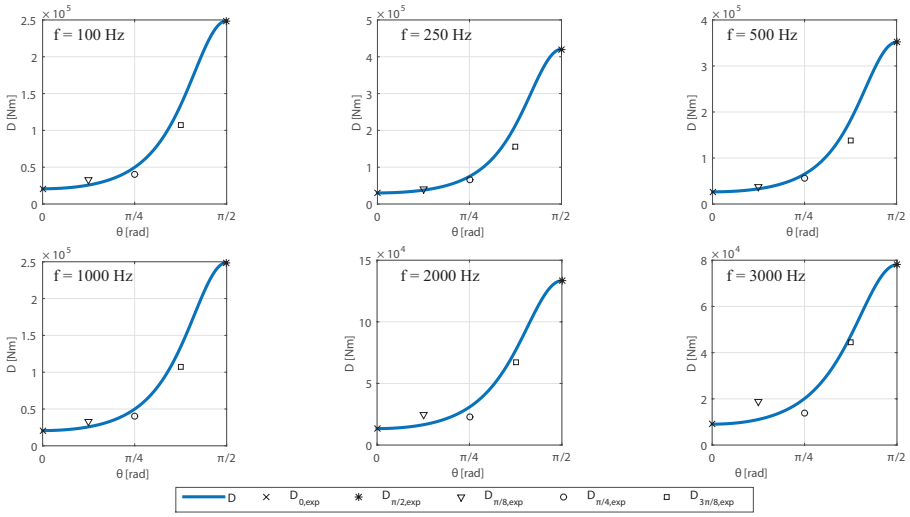

Figure 8: Elliptic model: comparison between the elliptic approximation and the experimental bending stiffness, determined for the angles: $\pi/8$, $\pi/4$ and $3\pi/8$; at the frequencies: 100 Hz; 200 Hz, 500 Hz, 1000 Hz, 200 Hz and 3000 Hz.

Lastly, the frequency and direction dependent apparent bending stiffness of the orthotropic cross-laminated timber plate is shown in Figure 9.

6. Conclusion

In this paper the elastic and stiffness characteristics of an orthotropic cross-laminated timber plate have been investigated as a function of the experimental flexural wave velocity. The real part of the wave velocity was evaluated using two different approaches. The phase difference method gives more accurate results in the low frequency range, while at high frequencies it is more convenient to determine the velocity from the time of flight difference, evaluated between neighbouring transducers. Using a non-linear fitting algorithm, the elastic E and the shear moduli G have been derived from the experimental wave velocities, measured along the plate's principal directions. Results show that the y-direction, in which the outer layers fibres are vertically oriented, is stiffer than the orthogonal x-direction. Moreover, the elastic modulus E_y is two orders of magnitude higher that the shear modulus G_{yz}, while along the x-direction the elastic and the shear moduli have a comparable order of magnitude.

Furthermore, the apparent stiffness properties of an equivalent thin CLT plate have been derived from the experimental flexural wavenumbers, using Kirchhoff's dispersion relation. The equivalent thin plate exhibits a frequency dependent bending stiffness, which compensates the fact that rotational inertia, shear effects, and the layered structure are neglected. The elastic modulus and the bending stiffness decrease as the frequency increases. The frequency dependence is much more emphasised along the $y-$direction due to the big difference between the elastic and the shear moduli. The stiffness properties, evaluated along the principal directions, are derived

Published article available online: https://doi.org/10.1016/j.jsv.2017.04.018

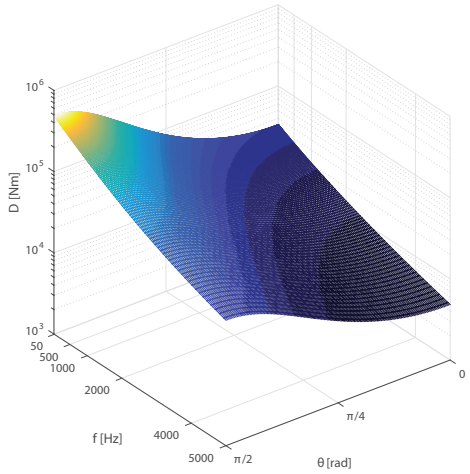

Figure 9: Apparent bending stiffness of an equivalent orthotropic thin CLT plate, frequency and direction dependent.

for each propagation angle by using an orthotropic elliptic model, which provides a good approximation of the experimental data within the considered frequency range. Although the classical thin plate theory does not rigorously describe the dynamic behaviour of the CLT structure, it is often used in vibro-acoustic analysis providing well approximated results.

The presented method allows one to quickly evaluate the elastic and stiffness properties of orthotropic building elements. Moreover, the data fitting using Mindlin's dispersion relation provides an efficient method that does not require a dense frequency sampling, reducing significantly the measurement time. The non-destructive nature of the test makes this method a suitable approach both for in-situ and laboratory applications. The main drawback of the method is the high influence of the measurement points spacing on the accuracy of experimental results. Especially at high frequencies, as the wavelength become shorter, a small uncertainty in the accelerometers spacing will increase the scatter of the results. The perfectly free propagating wave assumption, where both the evanescent near field and the reflections from the plate discontinuity can be neglected, is neither easy to obtain, nor to verify. Despite these uncertainties the method represents an useful tool to quickly investigate the stiffness properties of orthotropic structures that are usually required as input data in vibro-acoustic prediction models.

Acknowledgement

All the experimental measurements and most of the data analysis have been performed at *Empa - Swiss Federal Laboratories for Material Science and Technology - Laboratory for Acoustics/Noise Control*.

Published article available online: https://doi.org/10.1016/j.jsv.2017.04.018

Appendix A. Experimental results

In this section the flexural wave velocity measured along five propagation directions is presented. The propagation angles $0 \leq \theta \leq \pi/2$ were investigated at steps of $\pi/8$ radians. The inner core fibres are oriented along the principal x-direction, $\theta = 0$ while the outer layers fibres are vertically oriented along the principal y-direction, $\theta = \pi/2$. The velocities obtained from the phase difference method, and by evaluating the time of flight difference, are compared in the graph on the left-hand side: (a). The experimental data set, derived from the combination of these results by using a cut off frequency $f = 1500$ Hz, were fitted using Mindlin's wave dispersion relation, given Eq. (5), as shown in the graph on the right-hand side: (b).

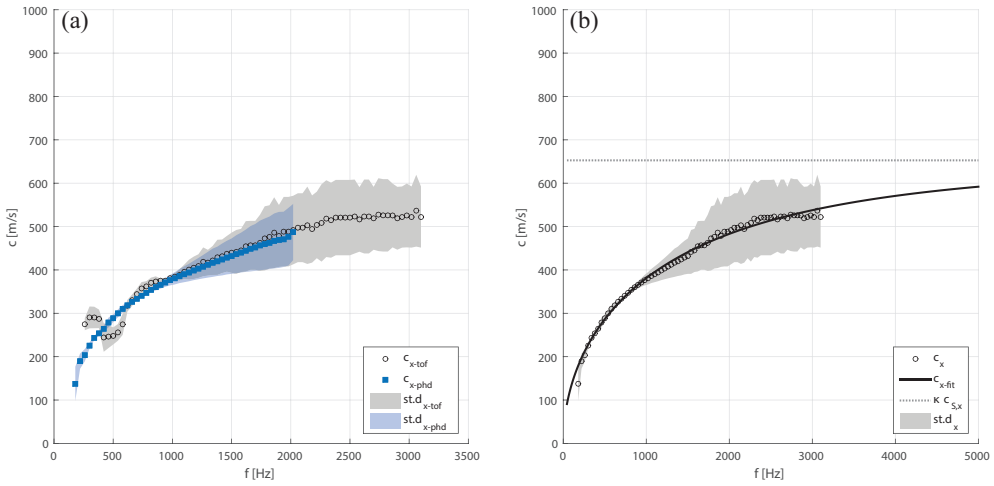

Figure A.10: (a) – Experimental wave velocity determined from the phase difference (*phd*) and the time of flight (*tof*) methods. (b) – Curve fitting of the experimental wave velocity using Mindlin's dispersion relation. The shaded area represents the standard deviation of measured data. Propagation angle: $\theta = 0$.

References

[1] EN ISO 16351 – Timber structures. Cross laminated timber. Requirements, Standard, International Organization for Standardization, Geneva, CH (2015).

[2] R. Öqvist, F. Ljunggren, A. Ågren, Variations in sound insulation in cross laminated timber housing construction, in: Proceedings of Forum Acusticum 2011, EAA, Aalborg, Denmark, June 2011.

[3] S. Schoenwald, B. Zeitler, I. Sabourin, F. King, Sound insulation performance of cross laminated timber building systems, in: Proceedings of the 42nd International Congress and Exposition on Noise Control Engineering, Institute of Noise Control Engineering, Innsbruck, Austria, September 2013.

[4] P. Niemz, D. Mannes, Non-destructive testing of wood and wood-based materials, Journal of Cultural Heritage 13 (3) (2012) S26–S34.

[5] P. S. Frederiksen, Experimental procedure and results for the identification of elastic constants of thick orthotropic plates, Journal of Composite Materials 31 (4) (1997) 360–382.

[6] E. O. Ayorinde, L. Yu, On the elastic characterization of composite plates with vibration data, Journal of Sound and Vibration 283 (1) (2005) 243–262.

Published article available online: https://doi.org/10.1016/j.jsv.2017.04.018

[7] V. Bucur, R. Archer, Elastic constants for wood by an ultrasonic method, Wood Science and Technology 18 (4) (1984) 255–265.
[8] D. Keunecke, W. Sonderegger, K. Pereteanu, T. Lüthi, P. Niemz, Determination of Young's and shear moduli of common yew and norway spruce by means of ultrasonic waves, Wood science and technology 41 (4) (2007) 309–327.
[9] U. Dackermann, R. Elsener, J. Li, K. Crews, A comparative study of using static and ultrasonic material testing methods to determine the anisotropic material properties of wood, Construction and Building Materials 102 (2016) 963–976.
[10] P. Bonfiglio, F. Pompoli, Determination of the dynamic complex modulus of viscoelastic materials using a time domain approach, Polymer Testing 48 (2015) 89–96.
[11] J. Rindel, Dispersion and absorption of structure-borne sound in acoustically thick plates, Applied Acoustics 41 (2) (1994) 97–111.
[12] T. Nightingale, R. Halliwell, G. Pernica, Estimating in-situ material properties of a wood joist floor: Part 1-measurements of the real part of bending wavenumber and modulus of elasticity, Building Acoustics 11 (3) (2004) 1–27.
[13] N. Clark, S. Thwaites, Local phase velocity measurements in plates, Journal of Sound and Vibration 187 (2) (1995) 241–252.
[14] S. Thwaites, N. Clark, Non-destructive testing of honeycomb sandwich structures using elastic waves, Journal of Sound and Vibration 187 (2) (1995) 253–269.
[15] D. Gsell, G. Feltrin, S. Schubert, R. Steiger, M. Motavalli, Cross-laminated timber plates: evaluation and verification of homogenized elastic properties, Journal of Structural Engineering 133 (1) (2007) 132–138.
[16] B. Van Damme, S. Schoenwald, M. Alvarez Blanco, A. Zemp, Limitation to the use of homogenized material parametrs of cross laminated timber plates for vibration and sound transmission modelling, in: Proceedings of the 22^{nd} International Congress on Sound and Vibration, International Institute of Acoustics and Vibration, Florence, Italy, July 2015.
[17] M. E. McIntyre, J. Woodhouse, On measuring the elastic and damping constants of orthotropic sheet materials, Acta Metallurgica 36 (6) (1988) 1397–1416.
[18] R. Stürzenbecher, K. Hofstetter, J. Eberhardsteiner, Structural design of cross laminated timber (CLT) by advanced plate theories, Composites Science and Technology 70 (9) (2010) 1368–1379.
[19] A. Santoni, S. Schoenwald, B. Van Damme, H. M. Trobs, P. Fausti, Average sound radiation model for orthotropic cross laminated timber plates., in: Proceedings of Euroregio 2016, EAA-SPA-SEA, Porto, Portugal, June 2016.
[20] S. S. Rao, Vibration of continuous systems, John Wiley & Sons, Inc., Hoboken, NJ, USA, 2007.
[21] R. D. Mindlin, Influence of rotary inertia and shear on flexural motions of isotropic elastic plates, Journal of Applied Mechanics 18 (1) (1951) 31–38.
[22] S. P. Timoshenko, X. on the transverse vibrations of bars of uniform cross-section, The London, Edinburgh, and Dublin Philosophical Magazine and Journal of Science 43 (253) (1922) 125–131.
[23] I. A. Viktorov, Rayleigh and Lamb waves: physical theory and applications, Plenum Press, New York, USA, 1967.
[24] K. F. Graff, Wave motion in elastic solids, Dover Publications, Inc., New York, USA, 1991.
[25] A. Nilsson, B. Liu, Vibro-acoustics, Vol. 2, Science Press, Beijing and Springer-Verlag, Berlin Heidelberg, 2015.
[26] L. Cremer, M. Heckl, B. A. T. Petersson, Structure-borne sound, 3rd Edition, Springer-Verlag, Berlin Heidelberg, 2005.
[27] I. Roelens, F. Nuytten, I. Bosmans, G. Vermeir, In situ measurement of the stiffness properties of building components, Applied Acoustics 52 (3) (1997) 289–309.
[28] J. Chung, T. Chung, K. Kim, Vibration analysis of orthotropic mindlin plates with edges elastically restrained against rotation, Journal of Sound and Vibration 163 (1) (1993) 151–163.
[29] A. W. Leissa, Vibration of plates, Tech. Rep. NASA SP-160, National Aeronautics and Space Administration, Washington, DC (1969).
[30] A. Nilsson, B. Liu, Vibro-acoustics, Vol. 1, Science Press, Beijing and Springer-Verlag, Berlin Heidelberg, 2015.
[31] R. Szilard, Theories and applications of plate analysis: classical numerical and engineering methods, John Wiley & Sons, Hoboken, NJ, USA, 2004.
[32] E. Piana, P. Milani, N. Granzotto, Simple method to determine the transmission loss of gypsum panels, in: Proceedings of the 21^{nd} International Congress on Sound and Vibration Proceedings, International Institute of Acoustics and Vibration, Beijing, China, 2015.
[33] J. Anderson, M. Bratos-Anderson, Radiation efficiency of rectangular orthotropic plates, Acta acustica united with acustica 91 (1) (2005) 61–76.
[34] J.-G. Richter, B. Zeitler, I. Sabourin, S. Schoenwald, Comparison of different methods to measure structural damping, Canadian Acoustics 39 (3) (2011) 54–55.
[35] T. Pritz, Frequency dependences of complex moduli and complex poisson's ratio of real solid materials, Journal of Sound and Vibration 214 (1) (1998) 83–104.

Published article available online: https://doi.org/10.1016/j.jsv.2017.04.018

[36] E. Nilsson, A. Nilsson, Prediction and measurement of some dynamic properties of sandwich structures with honeycomb and foam cores, Journal of sound and vibration 251 (3) (2002) 409–430.
[37] D. Backström, A. C. Nilsson, Modelling the vibration of sandwich beams using frequency-dependent parameters, Journal of Sound and Vibration 300 (3) (2007) 589–611.
[38] B. Van Damme, S. Schoenwald, A. Zemp, Modeling the bending vibration of cross-laminated timber beams, European Journal of Wood and Wood Products (2017) online 1–10.
[39] J. Bodig, B. A. Jayne, Mechanics of Wood and Wood Composites, Van Nostrand Reinhold Company, New York, USA, 1982.

Published article available online: https://doi.org/10.1016/j.jsv.2017.04.018

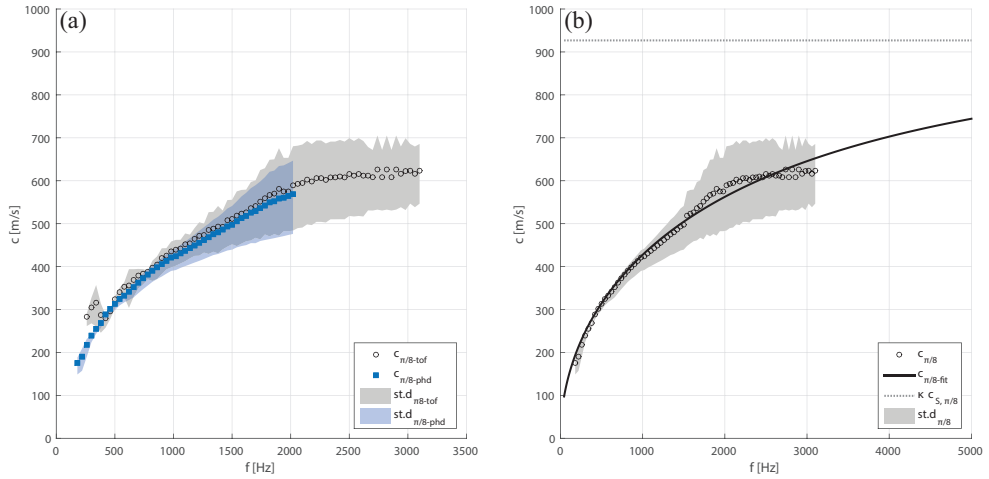

Figure A.11: (a) – Experimental wave velocity determined from the phase difference (*phd*) and the time of flight (*tof*) methods. (b) – Curve fitting of the experimental wave velocity using Mindlin's dispersion relation. The shaded area represents the standard deviation of measured data. Propagation angle: $\theta = \pi/8$.

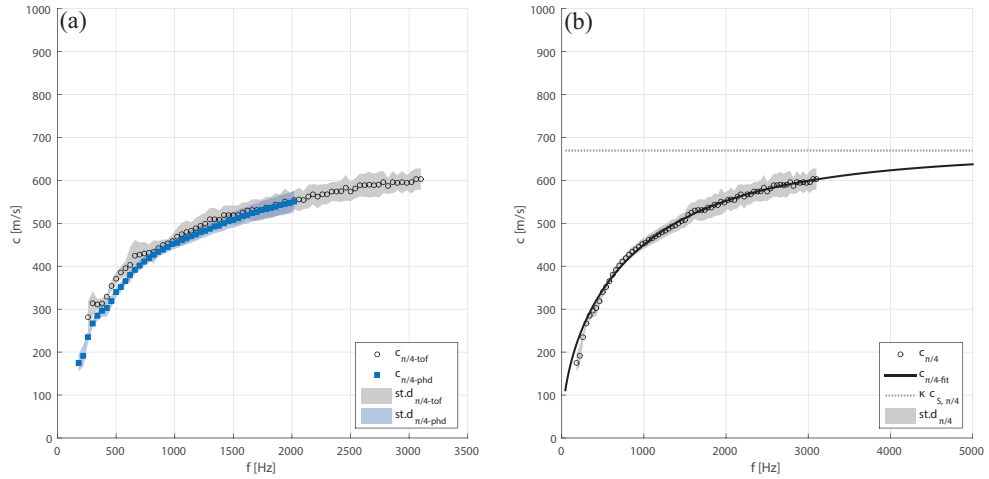

Figure A.12: (a) – Experimental wave velocity determined from the phase difference (*phd*) and the time of flight (*tof*) methods. (b) – Curve fitting of the experimental wave velocity using Mindlin's dispersion relation. The shaded area represents the standard deviation of measured data. Propagation angle: $\theta = \pi/4$.

Published article available online: https://doi.org/10.1016/j.jsv.2017.04.018

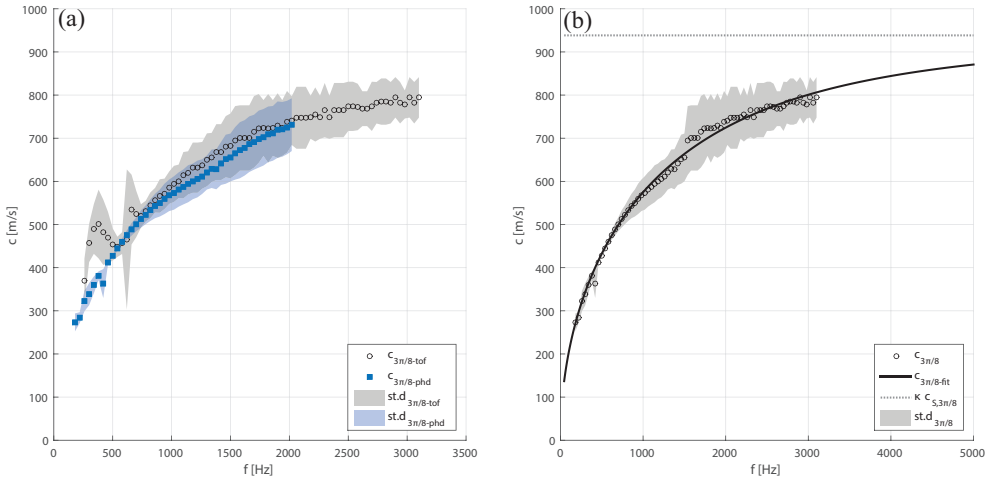

Figure A.13: (a) – Experimental wave velocity determined from the phase difference (*phd*) and the time of flight (*tof*) methods. (b) – Curve fitting of the experimental wave velocity using Mindlin's dispersion relation. The shaded area represents the standard deviation of measured data. Propagation angle: $\theta = 3\pi/8$.

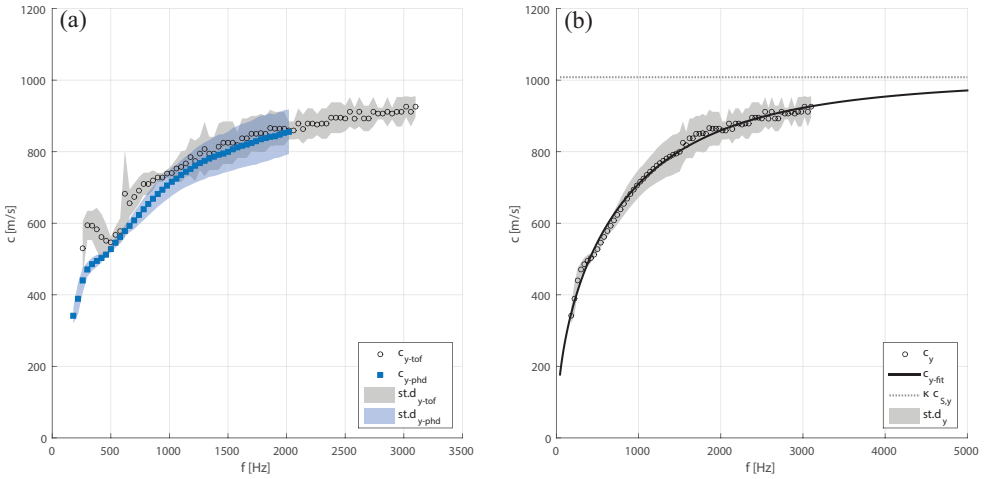

Figure A.14: (a) – Experimental wave velocity determined from the phase difference (*phd*) and the time of flight (*tof*) methods. (b) – Curve fitting of the experimental wave velocity using Mindlin's dispersion relation. The shaded area represents the standard deviation of measured data. Propagation angle: $\theta = \pi/2$.